Plasmonic Nonreciprocity Driven by Band Hybridization in Moiré Materials

Michał Papaj* and Cyprian Lewandowski*
Department of Physics, Massachusetts Institute of Technology, Cambridge, Massachusetts 02139, USA

(Received 29 January 2020; accepted 24 June 2020; published 5 August 2020)

We propose a new current-driven mechanism for achieving significant plasmon dispersion nonreciprocity in systems with narrow, strongly hybridized electron bands. The magnitude of the effect is controlled by the strength of electron-electron interactions α, which leads to its particular prominence in moiré materials, characterized by $\alpha \gg 1$. Moreover, this phenomenon is most evident in the regime where Landau damping is quenched and plasmon lifetime is increased. The synergy of these two effects holds great promise for novel optoelectronic applications of moiré materials.

DOI: 10.1103/PhysRevLett.125.066801

Introduction.—Time-reversal symmetry breaking leads to the emergence of unidirectional modes in platforms such as quantum Hall systems [1–3], quantum anomalous Hall materials [4–8], or topological photonic crystals [9–13]. However, such modes, while holding exceptional promise for the development of new devices, often require very specific experimental conditions, such as strong magnetic fields, significant magnetic impurity doping or a large, macroscopic size of a device. Frequently, such systems cannot be easily coupled to electromagnetic radiation, limiting their experimental utility. Moreover, they are not easily susceptible to the miniaturization necessary for technological applications, which usually benefit from nanoscale on-chip integration.

One of the alternative platforms in which nonreciprocity is highly sought after are 2D surface plasmons [14–26], collective charge density modes of fundamental importance in controlling light-matter interactions [27–29]. These quasiparticles can be excited using electromagnetic radiation and are an essential ingredient in developing optoelectronic devices. While nonreciprocity in the plasmon dispersion, $\omega_p(\mathbf{q}) \neq \omega_p(-\mathbf{q})$, can be induced using magnetic field [30–33], 2D plasmons also allow for an appealing alternative based on driving electric current through the devices—the so-called plasmonic Doppler effect [22–26,34]. The essence of this phenomenon boils down to a simple Galilean transformation that distinguishes plasmons moving along and against the electric current. Electron flow modifies the plasmon dispersion with a correction, $\Delta\omega_p^{(c)} \sim \mathbf{u}\cdot\mathbf{q}$, proportional to the drift velocity $\mathbf{u}$ and plasmon momentum $\mathbf{q}$. This current-induced nonreciprocity is the conventional plasmonic Doppler effect.

Unfortunately, even in pristine graphene samples, the drift velocity is a small fraction of Fermi velocity v_F [35,36]. Therefore, the relative magnitude of the Doppler effect [22],

$$\frac{\Delta\omega_p^{(c)}(\mathbf{q})}{\omega_p^0(\mathbf{q})} \sim \frac{1}{\alpha}\frac{u}{v_F}\frac{\omega_p^0(\mathbf{q})}{|\mu|}, \qquad \omega_p^0(\mathbf{q}) = \sqrt{4\alpha|\mu|v_F q}, \tag{1}$$

is a small correction on the order of ∼3% to the graphene plasmon dispersion in the absence of electron drift, $\omega_p^0(\mathbf{q})$ [37–41], as shown in Figs. 1(a), 1(b). Here $|\mu|$ is the Fermi energy and $\alpha = e^2/\hbar\kappa v_F$ characterizes the strength of the electronic interactions in a dielectric medium with a relative permittivity κ. Since in the most common scenarios $\alpha \sim 1$ (e.g., monolayer graphene), its presence in the drift-free part of the plasmon dispersion means that $\omega_p^0(\mathbf{q}) < |\mu|$, which is an additional limitation in the attempts to observe the conventional Doppler effect.

Here we show that strongly hybridized, narrow band materials characterized by $\alpha \gg 1$, can host a new, fundamentally quantum in nature, source of plasmonic nonreciprocity. In such a case, the asymmetry of the plasmon dispersion [as demonstrated in Figs. 1(c), 1(d)] is strongly enhanced by an additional factor of α:

$$\Delta\omega_p^{(q)}(\mathbf{q}) \sim \alpha\frac{\Delta_h^2 v_F q}{|\mu|^3}\mathbf{u}\cdot\mathbf{q}, \qquad \frac{\Delta\omega_p^{(q)}(\mathbf{q})}{\omega_p^0(\mathbf{q})} \sim \frac{u}{v_F}\frac{\Delta_h^2\omega_p^0(\mathbf{q})}{|\mu|^3}\frac{q}{k_F}, \tag{2}$$

where Δ_h is the strength of hybridization between the two bands that opens up a gap between them [see Fig. 2(a)]. Here, the relative frequency shift is amplified by the effective fine structure factor α unlike in the conventional Doppler effect $\Delta\omega_p^{(c)}(\mathbf{q})$. The origin of this new effect can be traced back to the hybridization effects in electronic band structure. When plasmon frequencies exceed the chemical potential, a regime guaranteed by the strong interactions $\alpha \gg 1$ [42], the new mechanism dominates over the conventional one, leading to a strong enhancement of plasmonic nonreciprocity.

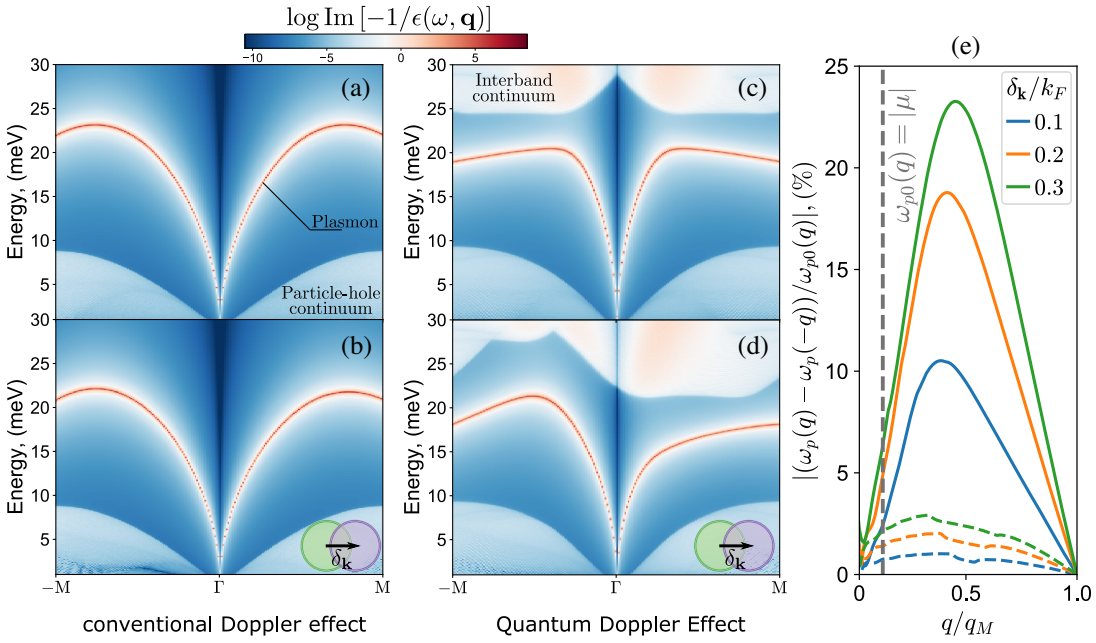

FIG. 1. (a)–(d) Electron loss functions of the narrow band tight-binding models. (a), (b) Unhybridized band model (a) without and (b) with electric current at $T = 0$. The conventional Doppler effect imposes only a small change on the plasmon dispersion. (c), (d) Hybridized band model (c) without and (d) with electric current at $T = 0$. Quantum Doppler effect results in a strong plasmon dispersion asymmetry. (e) A comparison of relative dispersion asymmetry at several drift velocity values. In a hybridized system (solid) strong asymmetry develops, which is purely a consequence of a nonvanishing interband wave function overlap, in contrast to an unhybridized system showing only a conventional Doppler effect (dashed). Here q_M is the length of the $\Gamma - M$ vector of the moiré Brillouin zone.

While this new source of band structure-driven nonreciprocity is a general consequence of band hybridization, the necessary ingredient ensuring a drastic increase in the effect's magnitude is the presence of strong electron-electron interactions. A natural platform with these attributes are the moiré materials, such as the twisted bilayer graphene (TBG) [43–45] or the *ABC* stacked trilayer graphene (TLG) [46]. This enhancement of electron-electron interactions is due to the emergence of a superlattice with a period much larger than the atomic spacing of the original crystal. Such a large lattice constant results in a small Brillouin zone, giving rise to a set of extremely narrow minibands with bandwidths on the order of tens of meV [47,48]. Therefore, moiré materials are in many ways an ideal realization of a strongly correlated system: the same sample can display a record-low density superconductivity [44,45,49], a correlated insulating state [43,46,50], or an interaction-driven ferromagnetism [51,52]. These narrow bands also offer a key advantage to plasmonics: narrow-band plasmons can rise above the particle-hole continuum, thus quenching Landau damping [42,53]. These characteristics make moiré materials a perfect platform to realize nonreciprocal plasmons with long lifetimes.

In this work we focus specifically on TLG as it features a single separated flatband that can be tuned using an external electric field [46,49]. We employ a continuum model [46,54,55] to perform a material-realistic calculation of the plasmon dispersion. These simulations show a significant plasmonic nonreciprocity, exceeding that predicted due to the conventional plasmon Doppler effect, and thus demonstrating moiré materials as a promising optoelectronics platform.

Minimal band structure model.—To elucidate the microscopic origins of the new nonreciprocity mechanism, we develop a minimal model capturing the essential features of the complicated moiré band structures relevant to the plasmonic Doppler effect. We use a toy-model Hamiltonian $H = H_0 + H_d + H_h$, where

$$H_0 = \frac{k^2}{2m}\sigma_z, \qquad H_d = \Delta_d \sigma_z, \qquad H_h = \Delta_h \sigma_x. \quad (3)$$

H_0 consists of two parabolic bands that can be thought of as coming from a tight-binding model. Here m is the effective mass large enough such that the plasmons extend above the intraband particle-hole continuum of each band, and $\sigma_{x,y,z}$ are the Pauli matrices. To describe the energy gap separating the flatband from the rest of the moiré minibands, we use two mechanisms: H_d, a trivial displacement-field-like gap, and H_h, a band hybridization term. We label the electron energies and their Bloch eigenstates as $E_{s,\mathbf{k}}$ and $\psi_{s,\mathbf{k}}$, respectively, with a schematic band structure shown in Fig. 2(a). We place the Fermi energy μ inside the valence band so that it qualitatively corresponds to the flatband of TLG.

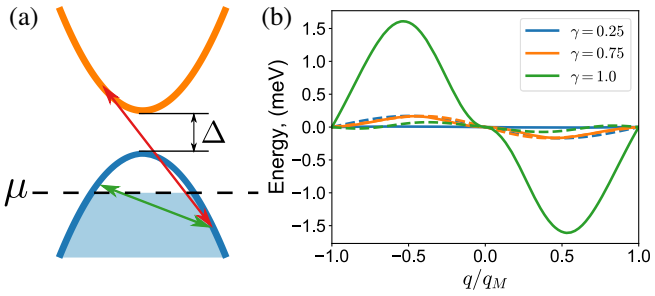

FIG. 2. (a) The polarization function contribution of the interband transitions (red), unlike that of the intraband transitions (green), is suppressed for ω smaller than the band gap $\Delta = 2\sqrt{\Delta_d^2 + \Delta_h^2}$. (b) Shift of the plasmon dispersion obtained from the tight-binding model due to the quantum (solid) and the conventional (dashed) Doppler effect for different degrees of band hybridization γ. Here $\Delta_h = \gamma\Delta$ and $\Delta_d = \sqrt{1-\gamma^2}\Delta$ to keep the gap Δ constant.

Plasmons in narrow-band materials.—Collective charge modes correspond to the nodes of the dynamical dielectric function $\varepsilon(\omega, \mathbf{q}) = 1 - V_{\mathbf{q}}\Pi(\omega, \mathbf{q})$, where $V_{\mathbf{q}} = 2\pi e^2/\kappa q$ is the Coulomb potential. We calculate the electron polarization function $\Pi(\omega, \mathbf{q})$ within the random phase approximation [56]

$$\Pi(\omega, \mathbf{q}) = 4\sum_{\mathbf{k},s,s'} \frac{(f_{s,\mathbf{k}+\mathbf{q}} - f_{s',\mathbf{k}})F^{ss'}_{\mathbf{k}+\mathbf{q},\mathbf{k}}}{E_{s,\mathbf{k}+\mathbf{q}} - E_{s',\mathbf{k}} - \omega - i0}, \tag{4}$$

where $\sum_{\mathbf{k}}$ denotes integration over the Brillouin zone and the indices s, s' run over electron bands. The factor of 4 accounts for the fourfold spin and valley degeneracy mimicking the degeneracy of the TLG superlattice. Here $f_{s,\mathbf{k}}$ is the Fermi-Dirac distribution, and $F^{ss'}_{\mathbf{k}+\mathbf{q},\mathbf{k}} = |\langle\psi_{s,\mathbf{k}+\mathbf{q}}|\psi_{s',\mathbf{k}}\rangle|^2$ describes the overlap between the Bloch eigenstates.

Origins of plasmonic nonreciprocity.—We now focus on explaining the behavior of the plasmon modes in this toy model with an electron carrier drift present in the system. As the interband terms in the polarization function will be suppressed by the large denominator on the order of the band gap energy scale, it is therefore sufficient to focus only on the intraband contribution. To that end we expand the intraband term in powers of $1/\omega$ to obtain

$$\Pi(\omega, \mathbf{q}) \approx \frac{A_1(\mathbf{q})}{\omega} + \frac{A_2(\mathbf{q})}{\omega^2} + \frac{A_3(\mathbf{q})}{\omega^3} + \cdots. \tag{5}$$

The coefficients in the above expansion are

$$A_n(\mathbf{q}) = 4\sum_{\mathbf{k}} \tilde{f}_{\mathbf{k}}(F^{--}_{\mathbf{k},\mathbf{k}+\mathbf{q}}\Delta E^{n-1}_{\mathbf{k}+\mathbf{q},\mathbf{k}} - F^{--}_{\mathbf{k},\mathbf{k}-\mathbf{q}}\Delta E^{n-1}_{\mathbf{k},\mathbf{k}-\mathbf{q}}), \tag{6}$$

with $\Delta E^n_{\mathbf{k},\mathbf{k}'} \equiv (E_{-,\mathbf{k}} - E_{-,\mathbf{k}'})^n$ corresponding to the nth power of the energy difference of the intraband transitions, and $\tilde{f}_{\mathbf{k}} \equiv f_{-,\mathbf{k}-m\mathbf{u}}$ denoting the drift-modified distribution function as described in the Supplemental Material [57]. These expressions rely on the Fermi energy μ placement in the valence band $s = -$ and hence the conduction band being completely unoccupied at low temperatures.

Now we analyze the most insightful regime of $|\mu| \gg \Delta_d, \Delta_h$. We expand the band overlap factors and the energy differences in the small-q limit and then focus only on the leading $\mathbf{k}$ behavior of $A_n(\mathbf{q})$. We begin with the $A_1(\mathbf{q})$ coefficient, obtaining

$$A_1(\mathbf{q}) \approx -\frac{2}{\pi}\frac{\Delta_h^2 u q^3 \cos(\theta_u)}{|\mu|^3}, \tag{7}$$

where we approximated the Fermi energy as $|\mu| \approx k_F^2/2m$ and θ_u is the angle between $\mathbf{q}$ and $\mathbf{u}$. As expected, in the absence of drift current, $\mathbf{u} = 0$, the time-reversal symmetry is preserved and the odd $1/\omega$ powers in expansion of $\Pi(\omega, \mathbf{q})$ vanish [58]. Furthermore, if there is no hybridization between the bands, $\Delta_h = 0$, the $1/\omega$ contribution to the polarization clearly vanishes.

Following the same approach, we now evaluate $A_2(\mathbf{q})$ and $A_3(\mathbf{q})$. To the leading order in $\mathbf{q}$ we can set the band overlap factors in Eq. (6) as unity, finding

$$A_2(\mathbf{q}) \approx \frac{2}{\pi}|\mu|q^2, \qquad A_3(\mathbf{q}) \approx -\frac{4}{\pi}u\cos\theta_u|\mu|q^3. \tag{8}$$

The q dependence of the $A_n(\mathbf{q})$ coefficients is easily understood. This is because the lowest possible contribution to the polarization function is always of the order $\sim q^2$ [56] and thus the first term that can be an odd function of the angle $\cos(\theta_u)$ has to scale as q^3.

We are now in a position to obtain the plasmon dispersion $\omega_p(\mathbf{q})$ using the cubic equation

$$0 = \omega^3 - \frac{2\pi\alpha v_F}{q}[A_1(\mathbf{q})\omega^2 + A_2(\mathbf{q})\omega + A_3(\mathbf{q})], \tag{9}$$

with $v_F = k_F/m$. Solving this equation perturbatively in the powers of the electron drift velocity u we find the plasmon dispersion as

$$\omega_p(\mathbf{q}) \approx \sqrt{4\alpha|\mu|v_F q} - 2\alpha\frac{\Delta_h^2 v_F q}{|\mu|^3}\mathbf{u}\cdot\mathbf{q} - \mathbf{u}\cdot\mathbf{q}, \tag{10}$$

which is the central result of our work. It is the last two terms in the above expression that are behind the plasmonic nonreciprocity in the presence of electron drift.

Quantum Doppler effect.—The second term in Eq. (10) is the new source of plasmonic nonreciprocity, which dominates in narrow-band materials. To see this we analyze the system parameters' dependence of the Doppler corrections.

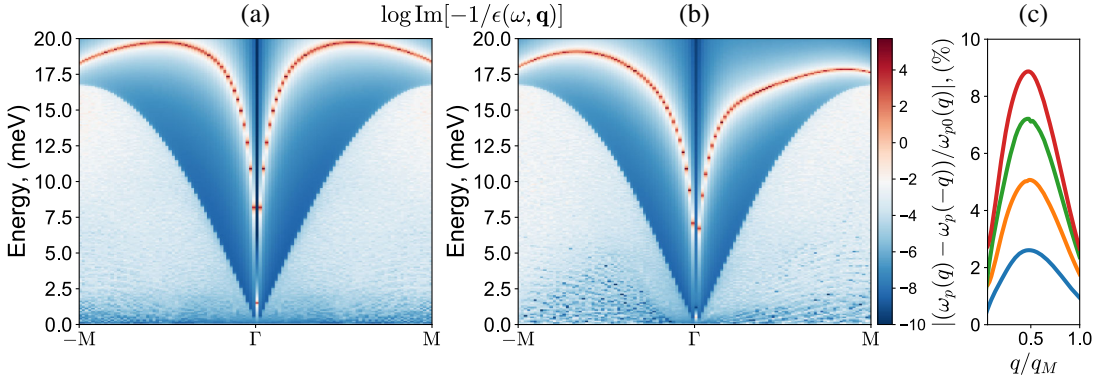

FIG. 3. Electron loss function in TLG (a) without and (b) with an applied electric current. The plasmon dispersion exhibits strong nonreciprocity under the Fermi surface shift $\delta_{\mathbf{k}} = 0.2q_M$. (c) Relative nonreciprocity for several values of $\delta_{\mathbf{k}} = cq_M$, with $c = 0.05$, 0.1, 0.15, 0.2 and $q_M = 0.24$ nm^{-1}.

The conventional Doppler shift (last term) depends only on the drift velocity u and thus its magnitude is only weakly tunable. For $q \sim k_F$ it is a fraction of the chemical potential,

$$\Delta\omega_p^{(c)} \approx uk_F \approx \frac{u}{v_F}|\mu|, \qquad |\mu| \approx v_F k_F, \tag{11}$$

as the drift velocity u is always smaller than the Fermi velocity v_F. This contrasts the quantum contribution, the second term in Eq. (10), where the effect's magnitude can be drastically increased by effective fine-structure constant α. At momenta $q \sim k_F$ it is

$$\Delta\omega_p^{(q)} \approx 2\alpha\frac{u}{v_F}\frac{\Delta_h^2 v_F^2 k_F^2}{|\mu|^3} \approx 2\alpha\frac{u}{v_F}\frac{\Delta_h^2}{|\mu|}, \tag{12}$$

and thus a large α offers a parametric increase of the effect. This is exactly the behavior we expect in narrow-electron band systems where $\alpha \gg 1$.

To further demonstrate this point we perform numerical calculations based on the narrow-band tight-binding model described in the Supplemental Material [57]. The plasmonic dispersion in the absence of the electric current is shown in Figs. 1(a), 1(c) for two parameter regimes: one with strongly hybridized bands due to the Δ_h term, and the other with decoupled bands simply displaced by a finite energy Δ_d. In both scenarios the parameters are chosen to keep the same bandwidth and band gap of 10 meV. Both cases exhibit qualitatively similar behavior—plasmons' dispersions settle between the intra- and interband particle-hole continua as guaranteed by $\alpha \gg 1$ [42]. However, when electric current is introduced, the striking difference between them is immediately apparent. While in the unhybridized case the observed nonreciprocity is minute, Fig. 1(b), in the system with hybridized bands a strong asymmetry in plasmon dispersion arises, see Fig. 1(d). The nonreciprocity can be quantified by the dispersion asymmetry between the $\mathbf{q}$ and $-\mathbf{q}$ modes $[\omega_p(\mathbf{q}) - \omega_p(-\mathbf{q})]/\omega_p^0(\mathbf{q})$, displayed in Fig. 1(e) for both cases. While the conventional effect is present in both cases, the calculation in a strongly hybridized system reveals a remarkable, order of magnitude enhancement over the unhybridized one in agreement with the analytical calculation. This comparison between the conventional and the quantum Doppler effect is further exemplified by the crossover from the strongly to weakly hybridized system shown in Fig. 2(b). We vary the degree of band hybridization γ while keeping constant the bandwidths and band gaps, and plot $\Delta\omega_p^{(c)} = A_3/2A_2$ and $\Delta\omega_p^{(q)} = \pi\alpha v_F A_1/q$, with the latter clearly dominating when the bands are strongly hybridized.

We highlight that the $A_1(\mathbf{q})$ term responsible for the quantum Doppler effect is not just a special feature of our model, but rather is universal to any system with hybridized bands. In fact, the $1/\omega$ term appears also in the graphene Doppler shift calculations [22,25], but because the relevant plasmon frequencies are smaller or comparable to the Fermi energy $\omega_p \lesssim |\mu|$, the $A_1(\mathbf{q})$ term is suppressed by a small ratio of q^2/k_F^2. More generally, the origins of the $A_1(\mathbf{q})$ coefficient stem from a finite difference of the band overlap functions. This overlap measures the extent to which wave functions' spectral weight at different momenta come from the same bands. It is strongly dependent on the band hybridization and reaches unity far from the band crossing points as $|\mu|$ becomes larger. Indeed it is the relation between the chemical potential and the plasmon frequency which determines the crossover to the regime in which quantum contribution dominates,

$$\Delta\omega_p^{(q)}(\mathbf{q}) \gtrsim \Delta\omega_p^{(c)}(\mathbf{q}) \Rightarrow \omega_p^0(\mathbf{q}) \gtrsim |\mu|, \tag{13}$$

as indicated in the Fig. 1(e).

Doppler effect in moiré materials.—We turn now to a particular material realization of this phenomenon—*ABC* stacked trilayer graphene. To obtain electron bands and Bloch wave functions we perform a realistic material calculation using the continuum model introduced in Refs. [46,49,54,55,57]. With that model we numerically

evaluate the dielectric function and determine the resulting plasmon dispersion.

Figures 3(a), 3(b) demonstrate the plasmon dispersion in TLG without and with electric current, respectively. As in the tight binding model, an asymmetry $\omega_p(\mathbf{q}) \neq \omega_p(-\mathbf{q})$ develops due to the flowing electric current. In analyzing this figure it is insightful to compare it with the Figs. 1(c), 1(d) which reproduce qualitative features of the TLG calculation. Most crucially, we see a plasmon mode that rises above the particle-hole continuum and once the mode $\omega_p(\mathbf{q})$ exceeds the Fermi energy $|\mu|$ a strong nonreciprocity in its dispersion develops. This behavior is to be expected on the basis of the analysis leading to Eq. (13).

In Fig. 3(c) we see by evaluating the nonreciprocity measure that even for a realistic band structure and drift velocities the induced nonreciprocity is a significant correction to the plasmon dispersion exceeding conventional Doppler effect predictions. We underline again that the enhancement of the Doppler effect from Eq. (2) is a general feature of systems with narrow, strongly hybridized bands and thus not limited to TLG—we expect it to be present, and perhaps be even more pronounced, in other materials with these characteristics.

Summary and outlook.—A key feature shared by many moiré materials is their remarkable flat electron bands with extremely low Fermi velocity and, therefore, exceptionally large effective fine structure constant α values. In this work we showed how such strong interactions can lead to a new, significant source of plasmon nonreciprocity. Our results have immediate consequences of both practical and fundamental importance. First of all, they open a pathway to development of optoelectronic devices with suppressed backscattering [9,59–62], for example, plasmonic isolators based on Mach-Zehnder interferometers [63,64], making them a valuable addition to the nanophotonics toolbox. Moreover, the drift-based mechanism enables a highly tunable electrical control of nonreciprocity on a nanoscale by simply controlling the current flow in the device. This on-chip compactness and tunability are in striking contrast to the mechanisms that employ the magnetic-based approaches. Finally, introducing a nonreciprocity to the dispersion of plasmons with quenched Landau damping is particularly appealing, as it paves a way towards a practical realization of various theoretical predictions, such as the Dyakonov-Shur instability [34], that were previously limited by the plasmonic lifespan. As the collective modes in the moiré materials are actively searched for using near-field optical microscopy techniques [65–68], this work can open new prospects for both fundamental and practical applications of moiré plasmons.

We thank Leonid Levitov for drawing our attention to the concept of the plasmonic Doppler effect and Ali Fahimniya for useful discussions. M. P. was supported by DOE Office of Basic Energy Sciences under Award DE-SC0018945. C. L. acknowledges support from the MIT Physics graduate program and the STC Center for Integrated Quantum Materials, NSF Grant No. DMR-1231319.

*These authors contributed equally to this work.

[1] K. v. Klitzing, G. Dorda, and M. Pepper, New Method for High-Accuracy Determination of the Fine-Structure Constant Based on Quantized Hall Resistance, Phys. Rev. Lett. **45**, 494 (1980).
[2] B. I. Halperin, Quantized hall conductance, current-carrying edge states, and the existence of extended states in a two-dimensional disordered potential, Phys. Rev. B **25**, 2185 (1982).
[3] A. H. MacDonald and P. Středa, Quantized hall effect and edge currents, Phys. Rev. B **29**, 1616 (1984).
[4] F. D. M. Haldane, Model for a Quantum Hall Effect without Landau Levels: Condensed-Matter Realization of the "Parity Anomaly", Phys. Rev. Lett. **61**, 2015 (1988).
[5] R. Yu, W. Zhang, H.-J. Zhang, S.-C. Zhang, X. Dai, and Z. Fang, Quantized anomalous hall effect in magnetic topological insulators, Science **329**, 61 (2010).
[6] K. Nomura and N. Nagaosa, Surface-Quantized Anomalous Hall Current and the Magnetoelectric Effect in Magnetically Disordered Topological Insulators, Phys. Rev. Lett. **106**, 166802 (2011).
[7] Q.-Z. Wang, X. Liu, H.-J. Zhang, N. Samarth, S.-C. Zhang, and C.-X. Liu, Quantum Anomalous Hall Effect in Magnetically Doped Inas/Gasb Quantum Wells, Phys. Rev. Lett. **113**, 147201 (2014).
[8] C.-Z. Chang *et al.*, Experimental observation of the quantum anomalous hall effect in a magnetic topological insulator, Science **340**, 167 (2013).
[9] T. Ozawa, H. M. Price, A. Amo, N. Goldman, M. Hafezi, L. Lu, M. C. Rechtsman, D. Schuster, J. Simon, O. Zilberberg, and I. Carusotto, Topological photonics, Rev. Mod. Phys. **91**, 015006 (2019).
[10] L. Lu, J. D. Joannopoulos, and M. Soljačić, Topological photonics, Nat. Photonics **8**, 821 (2014).
[11] L. Lu, J. D. Joannopoulos, and M. Soljačić, Topological states in photonic systems, Nat. Phys. **12**, 626 (2016).
[12] A. B. Khanikaev and G. Shvets, Two-dimensional topological photonics, Nat. Photonics **11**, 763 (2017).
[13] X.-C. Sun, C. He, X.-P. Liu, M.-H. Lu, S.-N. Zhu, and Y.-F. Chen, Two-dimensional topological photonic systems, Prog. Quantum Electron. **55**, 52 (2017).
[14] K. Y. Bliokh, F. J. Rodríguez-Fortuño, F. Nori, and A. V. Zayats, Spin–orbit interactions of light, Nat. Photonics **9**, 796 (2015).
[15] J. C. W. Song and M. S. Rudner, Chiral plasmons without magnetic field, Proc. Natl. Acad. Sci. U.S.A. **113**, 4658 (2016).
[16] L.-k. Shi and J. C. W. Song, Plasmon Geometric Phase and Plasmon Hall Shift, Phys. Rev. X **8**, 021020 (2018).
[17] A. Kumar, A. Nemilentsau, K. H. Fung, G. Hanson, N. X. Fang, and T. Low, Chiral plasmon in gapped dirac systems, Phys. Rev. B **93**, 041413(R) (2016).

[18] A. Principi, M. I. Katsnelson, and G. Vignale, Edge Plasmons in Two-Component Electron Liquids in the Presence of Pseudomagnetic Fields, Phys. Rev. Lett. **117**, 196803 (2016).
[19] D. Jin, L. Lu, Z. Wang, C. Fang, J. D. Joannopoulos, M. Soljačić, L. Fu, and N. X. Fang, Topological magnetoplasmon, Nat. Commun. **7**, 13486 (2016).
[20] D. Jin, T. Christensen, M. Soljačić, N. X. Fang, L. Lu, and X. Zhang, Infrared Topological Plasmons in Graphene, Phys. Rev. Lett. **118**, 245301 (2017).
[21] Z. Yu, G. Veronis, Z. Wang, and S. Fan, One-Way Electromagnetic Waveguide Formed at the Interface between a Plasmonic Metal under a Static Magnetic Field and a Photonic Crystal, Phys. Rev. Lett. **100**, 023902 (2008).
[22] D. S. Borgnia, T. V. Phan, and L. S. Levitov, Quasi-relativistic doppler effect and non-reciprocal plasmons in graphene, arXiv:1512.09044.
[23] B. Van Duppen, A. Tomadin, A. N. Grigorenko, and M. Polini, Current-induced birefringent absorption and non-reciprocal plasmons in graphene, 2D Mater. **3**, 015011 (2016).
[24] K. Y. Bliokh, F. J. Rodríguez-Fortuño, A. Y. Bekshaev, Y. S. Kivshar, and F. Nori, Electric-current-induced unidirectional propagation of surface plasmon-polaritons, Opt. Lett. **43**, 963 (2018).
[25] M. Sabbaghi, H.-W. Lee, T. Stauber, and K. S. Kim, Drift-induced modifications to the dynamical polarization of graphene, Phys. Rev. B **92**, 195429 (2015).
[26] T. A. Morgado and M. G. Silveirinha, Drift-induced unidirectional graphene plasmons, ACS Photonics **5**, 4253 (2018).
[27] A. N. Grigorenko, M. Polini, and K. S. Novoselov, Graphene plasmonics, Nat. Photonics **6**, 749. (2012).
[28] M. S. Tame, K. R. McEnery, Ş. K. Özdemir, J. Lee, S. A. Maier, and M. S. Kim, Quantum plasmonics, Nat. Phys. **9**, 329 (2013).
[29] W. L. Barnes, A. Dereux, and T. W. Ebbesen, Surface plasmon subwavelength optics, Nature (London) **424**, 824 (2003).
[30] D. C. Glattli, E. Y. Andrei, G. Deville, J. Poitrenaud, and F. I. B. Williams, Dynamical Hall Effect in a Two-Dimensional Classical Plasma, Phys. Rev. Lett. **54**, 1710 (1985).
[31] D. B. Mast, A. J. Dahm, and A. L. Fetter, Observation of Bulk and Edge Magnetoplasmons in a Two-Dimensional Electron Fluid, Phys. Rev. Lett. **54**, 1706 (1985).
[32] D. Heitmann, Two-dimensional plasmons in homogeneous and laterally microstructured space charge layers, Surf. Sci. **170**, 332 (1986).
[33] S. J. Allen, H. L. Störmer, and J. C. M. Hwang, Dimensional resonance of the two-dimensional electron gas in selectively doped GaAs/AlGaAs heterostructures, Phys. Rev. B **28**, 4875 (1983).
[34] M. Dyakonov and M. Shur, Shallow Water Analogy for a Ballistic Field Effect Transistor: New Mechanism of Plasma Wave Generation by dc Current, Phys. Rev. Lett. **71**, 2465 (1993).
[35] V. E. Dorgan, M.-H. Bae, and E. Pop, Mobility and saturation velocity in graphene on SiO_2, Appl. Phys. Lett. **97**, 082112 (2010).
[36] J. Yu, G. Liu, A. V. Sumant, V. Goyal, and A. A. Balandin, Graphene-on-diamond devices with increased current-carrying capacity: Carbon sp2-on-sp3 technology, Nano Lett. **12**, 1603 (2012).
[37] E. H. Hwang and S. D. Sarma, Dielectric function, screening, and plasmons in two-dimensional graphene, Phys. Rev. B **75**, 205418 (2007).
[38] B. Wunsch, T. Stauber, F. Sols, and F. Guinea, Dynamical polarization of graphene at finite doping, New J. Phys. **8**, 318 (2006).
[39] F. H. L. Koppens, D. E. Chang, and F. J. G. de Abajo, Graphene plasmonics: A platform for strong light–matter interactions, Nano Lett. **11**, 3370 (2011).
[40] M. Jablan, H. Buljan, and M. Soljačić, Plasmonics in graphene at infrared frequencies, Phys. Rev. B **80**, 245435 (2009).
[41] G. W. Hanson, Dyadic green's functions and guided surface waves for a surface conductivity model of graphene, J. Appl. Phys. **103**, 064302 (2008).
[42] C. Lewandowski and L. Levitov, Intrinsically undamped plasmon modes in narrow electron bands, Proc. Natl. Acad. Sci. U.S.A. **116**, 20869 (2019).
[43] Y. Cao, V. Fatemi, A. Demir, S. Fang, S. L. Tomarken, J. Y. Luo, J. D. Sanchez-Yamagishi, K. Watanabe, T. Taniguchi, E. Kaxiras, R. C. Ashoori, and P. Jarillo-Herrero, Correlated insulator behaviour at half-filling in magic-angle graphene superlattices, Nature (London) **556**, 80 (2018).
[44] Y. Cao, V. Fatemi, S. Fang, K. Watanabe, T. Taniguchi, E. Kaxiras, and P. Jarillo-Herrero, Unconventional superconductivity in magic-angle graphene superlattices, Nature (London) **556**, 43 (2018).
[45] M. Yankowitz, S. Chen, H. Polshyn, Y. Zhang, K. Watanabe, T. Taniguchi, D. Graf, A. F. Young, and C. R. Dean, Tuning superconductivity in twisted bilayer graphene, Science **363**, 1059 (2019).
[46] G. Chen, L. Jiang, S. Wu, B. Lyu, H. Li, B. L. Chittari, K. Watanabe, T. Taniguchi, Z. Shi, J. Jung, Y. Zhang, and F. Wang, Evidence of a gate-tunable Mott insulator in a trilayer graphene moiré superlattice, Nat. Phys. **15**, 237 (2019).
[47] R. Bistritzer and A. H. MacDonald, Moiré bands in twisted double-layer graphene, Proc. Natl. Acad. Sci. U.S.A. **108**, 12233 (2011).
[48] G. T. de Laissardière, D. Mayou, and L. Magaud, Numerical studies of confined states in rotated bilayers of graphene, Phys. Rev. B **86**, 125413 (2012).
[49] G. Chen, A. L. Sharpe, P. Gallagher, I. T. Rosen, E. J. Fox, L. Jiang, B. Lyu, H. Li, K. Watanabe, T. Taniguchi, J. Jung, Z. Shi, D. Goldhaber-Gordon, Y. Zhang, and F. Wang, Signatures of tunable superconductivity in a trilayer graphene moiré superlattice, Nature (London) **572**, 215 (2019).
[50] X. Lu, P. Stepanov, W. Yang, M. Xie, M. A. Aamir, I. Das, C. Urgell, K. Watanabe, T. Taniguchi, G. Zhang, A. Bachtold, A. H. MacDonald, and D. K. Efetov, Superconductors, orbital magnets and correlated states in magic-angle bilayer graphene, Nature (London) **574**, 653 (2019).
[51] A. L. Sharpe, E. J. Fox, A. W. Barnard, J. Finney, K. Watanabe, T. Taniguchi, M. A. Kastner, and D. Goldhaber-Gordon, Emergent ferromagnetism near three-quarters filling in twisted bilayer graphene, Science **365**, 605 (2019).
[52] M. Serlin, C. L. Tschirhart, H. Polshyn, Y. Zhang, J. Zhu, K. Watanabe, T. Taniguchi, L. Balents, and A. F. Young,

Intrinsic quantized anomalous hall effect in a moiré heterostructure, Science **367**, 900 (2020).
[53] K. Khaliji, T. Stauber, and T. Low, Plasmons and screening in finite-bandwidth 2d electron gas, arXiv:1910.01229.
[54] F. Zhang, B. Sahu, H. Min, and A. H. MacDonald, Band structure of ABC-stacked graphene trilayers, Phys. Rev. B **82**, 035409 (2010).
[55] M. Koshino and E. McCann, Trigonal warping and Berry's phase π in ABC-stacked multilayer graphene, Phys. Rev. B **80**, 165409 (2009).
[56] G. Mahan, *Many-Particle Physics* (Kluwer Academic/Plenum Publishers, New York, 2000).
[57] See Supplemental Material at http://link.aps.org/supplemental/10.1103/PhysRevLett.125.066801 for additional details of analytical derivation and numerical calculation.
[58] L. D. Landau and E. M. Lifshitz, *Electrodynamics of Continuous Media* (Pergamon, New York, 1984).
[59] S. Manipatruni, J. T. Robinson, and M. Lipson, Optical Nonreciprocity in Optomechanical Structures, Phys. Rev. Lett. **102**, 213903 (2009).
[60] A. Kamal, J. Clarke, and M. H. Devoret, Noiseless nonreciprocity in a parametric active device, Nat. Phys. **7**, 311 (2011).
[61] S. Hua, J. Wen, X. Jiang, Q. Hua, L. Jiang, and M. Xiao, Demonstration of a chip-based optical isolator with parametric amplification, Nat. Commun. **7**, 13657 (2016).
[62] D. Jalas, A. Petrov, M. Eich, W. Freude, S. Fan, Z. Yu, R. Baets, M. Popović, A. Melloni, J. D. Joannopoulos, M. Vanwolleghem, C. R. Doerr, and H. Renner, What is—and what is not—An optical isolator, Nat. Photonics **7**, 579 (2013).
[63] Z. Yu and S. Fan, Optical isolation based on nonreciprocal phase shift induced by interband photonic transitions, Appl. Phys. Lett. **94**, 171116 (2009).
[64] J. Fujita, M. Levy, R. M. Osgood, L. Wilkens, and H. Dötsch, Waveguide optical isolator based on mach–zehnder interferometer, Appl. Phys. Lett. **76**, 2158 (2000).
[65] J. Chen, M. Badioli, P. Alonso-González, S. Thongrattanasiri, F. Huth, J. Osmond, M. Spasenović, A. Centeno, A. Pesquera, P. Godignon, A. Z. Elorza, N. Camara, F. J. G. de Abajo, R. Hillenbrand, and F. H. L. Koppens, Optical nano-imaging of gate-tunable graphene plasmons, Nature (London) **487**, 77 (2012).
[66] Z. Fei, A. S. Rodin, G. O. Andreev, W. Bao, A. S. McLeod, M. Wagner, L. M. Zhang, Z. Zhao, M. Thiemens, G. Dominguez, M. M. Fogler, A. H. C. Neto, C. N. Lau, F. Keilmann, and D. N. Basov, Gate-tuning of graphene plasmons revealed by infrared nano-imaging, Nature (London) **487**, 82 (2012).
[67] F. Hu, S. R. Das, Y. Luan, T.-F. Chung, Y. P. Chen, and Z. Fei, Real-Space Imaging of the Tailored Plasmons in Twisted Bilayer Graphene, Phys. Rev. Lett. **119**, 247402 (2017).
[68] N. C. H. Hesp, I. Torre, D. Rodan-Legrain, P. Novelli, Y. Cao, S. Carr, S. Fang, P. Stepanov, D. Barcons-Ruiz, H. Herzig-Sheinfux, K. Watanabe, T. Taniguchi, D. K. Efetov, E. Kaxiras, P. Jarillo-Herrero, M. Polini, and F. H. L. Koppens, Collective excitations in twisted bilayer graphene close to the magic angle, arXiv:1910.07893.